THE JOURNAL OF BIOLOGICAL CHEMISTRY VOL. 281, NO. 41, pp. 30660–30668, October 13, 2006

Caveolar Endocytosis and Microdomain Association of a Glycosphingolipid Analog Is Dependent on Its Sphingosine Stereochemistry*[S]

Received for publication, June 28, 2006, and in revised form, July 31, 2006 Published, JBC Papers in Press, August 7, 2006, DOI 10.1074/jbc.M606194200

Raman Deep Singh[‡], Yidong Liu[§], Christine L. Wheatley[‡], Eileen L. Holicky[‡], Asami Makino[¶], David L. Marks[‡], Toshihide Kobayashi[¶], Gopal Subramaniam[§], Robert Bittman[§], and Richard E. Pagano[‡1]

From the [‡]Department of Biochemistry and Molecular Biology, Mayo Clinic College of Medicine, Rochester, Minnesota 55905, the [§]Department of Chemistry and Biochemistry, Queens College, The City University of New York, Flushing, New York 11367, and the [¶]RIKEN Frontier Research System, Wako, Saitama 351-0198, Japan

We have previously shown that glycosphingolipid analogs are internalized primarily via caveolae in various cell types. This selective internalization was not dependent on particular carbohydrate headgroups or sphingosine chain length. Here, we examine the role of sphingosine structure in the endocytosis of BODIPY^{TM}-tagged lactosylceramide (LacCer) analogs via caveolae. We found that whereas the LacCer analog with the natural (D-*erythro*) sphingosine stereochemistry is internalized mainly via caveolae, the non-natural (L-*threo*) LacCer analog is taken up via clathrin-, RhoA-, and Cdc42-dependent mechanisms and largely excluded from uptake via caveolae. Unlike the D-*erythro*-LacCer analog, the L-*threo* analog did not cluster in membrane microdomains when added at higher concentrations (5–20 μM). *In vitro* studies using small unilamellar vesicles and giant unilamellar vesicles demonstrated that L-*threo*-LacCer did not undergo a concentration-dependent excimer shift in fluorescence emission such as that seen with BODIPY^{TM}-sphingolipids with natural stereochemistry. Molecular modeling studies suggest that in D-*erythro*-LacCer, the disaccharide moiety extends above and in the same plane as the sphingosine hydrocarbon chain, while in L-*threo*-LacCer the carbohydrate group is nearly perpendicular to the hydrocarbon chain. Together, these results suggest that the altered stereochemistry of the sphingosine group in L-*threo*-LacCer results in a perturbed structure, which is unable to pack closely with natural membrane lipids, leading to a reduced inclusion in plasma membrane microdomains and decreased uptake by caveolar endocytosis. These findings demonstrate the importance of the sphingolipid stereochemistry in the formation of membrane microdomains.

Caveolar endocytosis occurs through flask-shaped invaginations at the plasma membrane (PM)[2] that are associated with the protein, caveolin-1. This internalization mechanism appears to be important in the cellular uptake and intracellular delivery of some bacteria, bacterial toxins, viruses, and circulating proteins (reviewed in Refs. 1–4). Caveolar endocytosis is cholesterol-sensitive, dynamin-dependent, and requires Src kinase activity (5–9). Markers used to visualize uptake through caveolae include labeled albumin (8, 10, 11), SV40 virus (12, 13), and in some cell types, the cholera toxin B (CtxB) subunit (8, 14–16). In addition to these markers, we have shown that fluorescently labeled lactosylceramide (BODIPY^{TM}-LacCer), and other glycosphingolipid (GSL) analogs, are internalized almost exclusively via caveolae in human skin fibroblasts (HSFs) and other cell types based on multiple approaches (7, 8, 11, 17). These include the use of pharmacological inhibitors and dominant negative (DN) proteins to selectively block particular mechanisms of endocytosis, as well as co-localization studies with various endocytic markers and with caveolin-1-fluorescent proteins.

The molecular basis for selective internalization of these GSL analogs via caveolae is unclear. We previously examined the effect of modifying the GSL carbohydrate head group but found no obvious difference in the internalization mechanism of fluorescent analogs of GalCer, LacCer, β-maltosylceramide (MalCer), globoside, sulfatide, and G_{M1} ganglioside (8). In the same study, we also varied the chain length of the sphingosine backbone (C_{12}, C_{16}, C_{18}, or C_{20}), the chain length of the BODIPY^{TM}-fatty acid, and the nature of the fluorophore used for synthesis of the LacCer analogs, but in each case the GSLs were internalized almost exclusively via caveolae. In the present study, we show that changing the sphingosine stereochemistry from the D to the L configura-

* This work was supported by National Institutes of Health Grants GM-22942 (to R. E. P.) and HL-083187 (to R. B.). The costs of publication of this article were defrayed in part by the payment of page charges. This article must therefore be hereby marked "*advertisement*" in accordance with 18 U.S.C. Section 1734 solely to indicate this fact.

[S] The on-line version of this article (available at http://www.jbc.org) contains supplemental Figs. 1–3 and two movies.

[1] To whom correspondence should be addressed: Dept. of Biochemistry and Molecular Biology, Mayo Clinic College of Medicine, 200 First St. SW, Rochester, MN 55905. Tel.: 507-284-8754; Fax: 507-266-4413; E-mail: pagano.richard@mayo.edu.

[2] The abbreviations used are: PM, plasma membrane; AF, Alexa Fluor; BODIPY^{TM}, boron dipyrromethenedifluoride; BODIPY^{TM}-LacCer, *N*-(4,4-difluoro-5,7-dimethyl-4-bora-3*a*,4*a*-diaza-*s*-indacene-3-pentanoyl)sphingosyl 1-β-D-lactoside; CtxB, cholera toxin B subunit; DN, dominant negative; D-*e*, D-*erythro*; D-*t*, D-*threo*; LacCer, β-lactosylceramide; GUV, giant unilamellar vesicle; HMEM, 10 mM HEPES-buffered minimal essential medium without indicator; HSF, human skin fibroblast; L-*e*, L-*erythro*; L-*t*, L-*threo*; PIPES, piperizine-1,4-bis(2-ethanesulfonic acid); POPC, 1-palmitoyl-2-oleoyl-*sn*-glycero-3-phosphocholine; SL, sphingolipid; SM, sphingomyelin; SUV, small unilamellar vesicle; Tfn, transferrin; GSL, glycosphingolipid; DOPC, dioleoylphosphatidylcholine; IL, interleukin; G_{M1}, Galβ1,3GalNAcβ1,4(Neu5Ac α2,3)Galβ1,4Glc β1,1′-ceramide.

tion inhibits LacCer uptake by caveolae and induces internalization by other endocytic mechanisms. In addition, evidence is presented showing that organization of the natural stereoisomer into PM microdomains is a prerequisite for its internalization through caveolae.

EXPERIMENTAL PROCEDURES

Cell Culture—Normal HSFs (GM- 5659) were obtained from Coriell Institute for Medical Research (Camden, NJ) and grown as described (18). All experiments were performed using monolayer cultures grown to ~35–50% confluence on acid-etched glass coverslips.

Lipids, Fluorescent Probes, and Miscellaneous Reagents—The non-natural D-*t*, L-*e*, and L-*t* stereoisomers of BODIPY™-LacCer, and the natural isomer, BODIPY™-D-*e*-LacCer, were synthesized and purified as described (18, 19). (2*S*)-3-Deoxy-BODIPY™-LacCer was synthesized as follows. After 1-pentadecyne was converted to (2*R*)-octadec-4-yne-1,2-diol (20), azidation with trimethylsilyl azide afforded (2*S*,4*Z*)-2-azido-octadec-4-en-1-ol (21), which was used as the lactosyl acceptor. Reaction with hepta-*O*-acetyl-β-lactosyl-1-trichloro-acetimidate (22) in methylene chloride in the presence of molecular sieves and a catalytic amount of boron trifluoride etherate, followed by hydrolysis of the acetate groups with sodium methoxide in methanol, provided (2*S*)-2-azido-3-deoxy-LacCer. Reduction of the azide with triphenylphosphine in aqueous tetrahydrofuran and *in situ N*-acylation with the *N*-hydroxysuccinimidoyl ester of 4,4-difluoro-5,7-dimethyl-4-bora-3a,4a-diaza-*s*-indacene-3-pentanoic acid (19) furnished the crude product, which was purified by column chromatography on silica gel followed by preparative thin-layer chromatography. The D-*e* and L-*t* isomers of BODIPY™-sphingomyelin (SM) were separated by thin-layer chromatography (23) using a commercial sample of BODIPY™-SM (Molecular Probes/Invitrogen; Eugene, OR) as the starting material. Each sphingolipid analog was complexed to defatted bovine serum albumin for incubation with cells (18). Fluorescent Alexa Fluor (AF) 594 or 647 labeled-transferrin (Tfn), AF594-dextran, and AF647-labeled anti-rabbit secondary antibodies were from Molecular Probes. Anti-β1-integrin (IgG1) antibodies were from Pharmingen (San Diego, CA). Anti-β1-integrin Fab fragments were generated from this IgG1 using the ImmunoPure IgG1 Fab preparation kit from Pierce and were labeled with AF647 succinimidyl ester using a protein labeling kit from Molecular Probes. All other reagents were from Sigma.

Protein Constructs and Co-transfections—Plasmids encoding wild type or DN AP180 (H. McMahon, Medical Research Council Laboratory of Molecular Biology), RhoA or Cdc42 (D. Billadeau, Mayo Foundation), or the IL-2R β chain (IL-2R β) (A. Dautry-Varsat, Institut Pasteur, Paris) were generous gifts as noted. For studies of protein overexpression, cells were co-transfected with the protein construct of interest and pDsRed2-Nuc (Clontech, Palo Alto, CA). The pDsRed2-Nuc construct labeled the nucleus with red fluorescence and served as a reporter for the transfected cells. Cells were transiently transfected using FuGENE 6 (Roche Diagnostics) and 3 μg/ml of DNA as described (8). Experiments were performed 24–48 h after transfection.

Incubation with Inhibitors—Cells were preincubated in HEPES-buffered MEM (HMEM) containing PP2 (EMD Biosciences, La Jolla, CA) (10 nM), genistein (50 μM), or *Clostridium difficile* toxin B (100 μM) for 1 h at 37 °C, or with nystatin (25 μg/ml) or chlorpromazine (8 μg/ml) for 30 min at 37 °C. Inhibitors were present in all subsequent steps of the experiment. Cells were then washed with ice-cold HMEM and incubated for 30 min at 10 °C with 2.5 μM BODIPY™-LacCer/bovine serum albumin to label the PM, washed twice with HMEM, and further incubated for 3 min at 37 °C, followed by back exchange with 5% defatted bovine serum albumin (6 times, 10 min each at 10 °C) to remove fluorescent lipid remaining at the PM after endocytosis (18). Samples were maintained at 10 °C and viewed under the fluorescence microscope (see below).

Incubation with Various Markers—Cells were incubated with 5 μg/ml AF594 Tfn for 30 min at 10 °C, further incubated for 3 min at 37 °C, and acid-stripped (8) to remove labeled protein remaining at the cell surface. For fluid phase uptake, cells were incubated with 1 mg/ml AF594-dextran for 5 min at 37 °C without preincubation or acid stripping. For IL-2R internalization studies, cells transiently transfected with IL-2R β were incubated with 1 nM IL-2 and 5 μg/ml phycoerythrin-mik-β3 (the IL-2R β chain antibody) for 5 min at 37 °C as described (17).

Microdomain Studies—HSFs were washed with ice-cold HMEM and transferred to 10 °C. Cells were incubated with the indicated concentration of BODIPY™-LacCer isomer for 30 min at 10 °C to label the PM. Samples were then washed, and images were acquired simultaneously at green and red wavelengths (see below). For specimens labeled with BODIPY™-lipid and AF647-Tfn or -Fab, images were acquired at three wavelengths (green, red, and far red) and subsequently rendered in pseudo color with *green* and *red* corresponding to LacCer and *blue* for the Tfn or Fab markers. All images were acquired on a cooled microscope stage maintained at 10 °C.

Fluorescence Microscopy and Analysis—Fluorescence microscopy was performed using an Olympus IX70 fluorescence microscope as described (7, 24). The microscope was equipped with a Dual-View module (Optical Insights; Tucson AZ) for simultaneous acquisition of green and red images. In experiments using double- or triple-labeled specimens, control samples were labeled identically with the individual fluorophores and exposed identically to the dual- or triple-labeled samples at each wavelength to verify that there was no crossover among emission channels. Digital images were quantified by image processing using Metamorph software (Molecular Devices, Sunnyvale, CA) as described (24, 25).

Lipid Vesicle Experiments—Small unilamellar vesicles (SUVs) were formed from 1-palmitoyl-2-oleoyl-*sn*-glycero-3-phosphocholine (POPC) and various amounts of BODIPY™-D-*e*- or L-*t*-LacCer (refer to Fig. 5) as described (26). Fluorescence scans of SUVs were performed using a Fluoromax-3 spectrofluorometer (HORIBA Jobin Yvon Inc., Edison, NJ). Giant unilamellar vesicles (GUVs) were prepared and examined by confocal fluorescence microscopy as described (27) with slight modifications. One ml of a chloroform solution containing 360 nmol of dioleoylphosphatidylcholine (DOPC), 20 nmol of dipalmitoylphosphatidylglycerol, 20 nmol of dilaur-

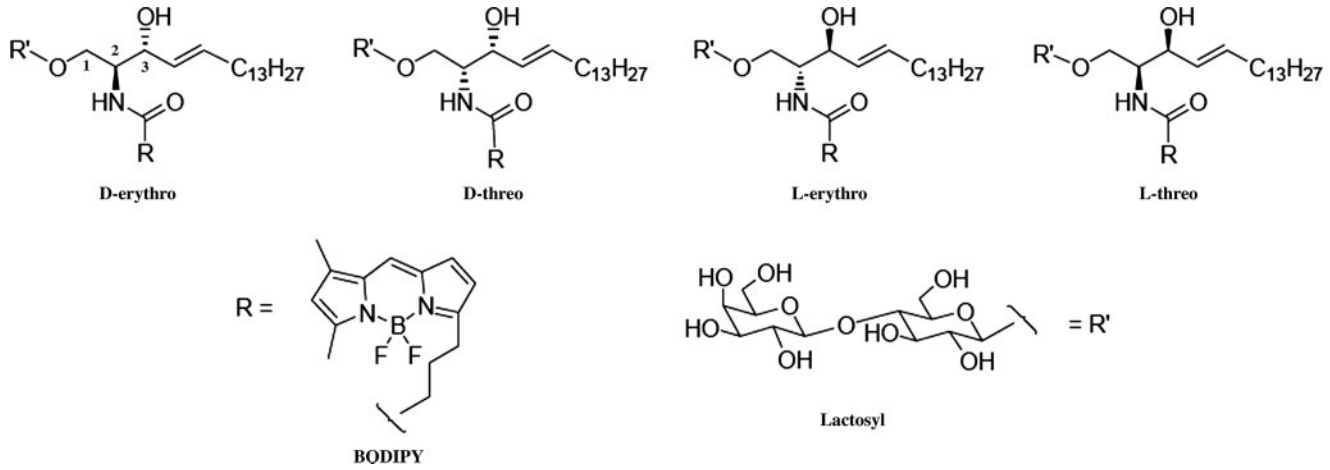

FIGURE 1. **Structures of BODIPY™-LacCer stereoisomers used in the current study.** Note that D-*erythro* is the naturally occurring stereochemistry for all SLs. Numbers on the D-*erythro* structure indicate the standard carbon numbering for sphingosine.

oylphosphatidylglycerol, and 40 nmol of BODIPY™-D-*e* or L-*t*-LacCer in a glass test tube was dried with a rotary evaporator to form a thin lipid film. The tubes were placed *in vacuo* for >2 h. After the completely dried lipid films were prehydrated with water-saturated nitrogen for 20 min at 50 °C, 1.6 ml of 5 mM PIPES buffer (pH 7.0) containing 50 mM KCl and 1 mM EDTA was added gently to the test tubes. The tubes were incubated at 55 °C overnight and then the samples were slowly cooled to room temperature. Harvested GUVs were placed on a coverslip and were enclosed on a slide glass within a ring of silicone high vacuum grease. The specimens were allowed to settle for 10 min. Fluorescence images were obtained with a Zeiss LSM 510 confocal microscope equipped with Plan-Apochromat 40×/1.2 water-corrected objective. Green fluorescence was observed by using a 488-nm argon laser for the excitation and a 505–530-nm filter for the emission. Red fluorescence was measured using the same excitation and a 560-nm cutoff filter for the emission.

Molecular Modeling Studies—Models of BODIPY™-LacCer stereoisomers were constructed and steric energy was minimized using the Chem3D program (Ultra 9.0, CambridgeSoft Corp., Cambridge, MA) with MM2 force field for removing van der Waals repulsions (28). This served to create the initial structures for calculating the ground-state equilibrium geometry by *ab initio* restricted Hartree-Fock methods (29) using the Spartan molecular modeling program for Windows (Spartan'04; Wavefunction Inc., Irvine, CA) on a desktop computer. Calculations were performed with the 3–21G* basis set (30) using the Pulay DIIS extrapolation (31) excluding solvent molecules for faster convergence.

RESULTS

Endocytosis Mechanism for the D- and L-Isomers of BODIPY™-LacCer Are Distinct—Our previous studies demonstrated that fluorescent analogs of LacCer and other GSLs are selectively internalized *via* caveolae in multiple cell types (7, 8, 11). These analogs all contained the natural, D-*erythro* (D-*e*) ceramide moiety. However, the ceramide moiety of all mammalian GSLs has two asymmetric carbon atoms and therefore four possible stereoisomers. In the present study, we synthesized all four stereoisomers of BODIPY™-LacCer (Fig. 1) and characterized their endocytosis in HSFs. The effect of various pharmacological inhibitors and DN AP180 on the internalization (3 min at 37 °C) of the different stereoisomers of BODIPY™-LacCer is shown in Fig. 2, *A* and *B*. Internalization of the D-*threo* (D-*t*) isomer was similar to that of the D-*e* isomer in that both were sensitive to treatments that inhibit caveolar uptake (nystatin, mβ-CD, genistein, or PP2) but were insensitive to inhibitors of clathrin-dependent endocytosis (chlorpromazine or DN AP180) (8, 17, 32). In contrast, the internalization of the L-*erythro* (L-*e*) and L-*threo* (L-*t*) isomers of BODIPY™-LacCer were also similar to each other but different from that seen using the D-isomers. Both of the L-isomers were inhibited ~70% by chlorpromazine or in cells expressing DN AP180, while little or no effect was seen using the other inhibitors. Additional studies were carried out using *Clostridium difficile* toxin B (toxin B) (a broad range Rho GTPase inhibitor that inhibits fluid phase endocytosis and phagocytosis (33, 34)), as well as DN constructs of RhoA and Cdc42 (Fig. 2, *C* and *D*). These treatments had little effect on the internalization of the BODIPY™-D-LacCer isomers but inhibited uptake of the L-*e* and L-*t* analogs by about 30–40% (Fig. 2, *C* and *D*).

Since both D-isomers behaved similarly to each other, and both L-isomers behaved similarly to each other, we restricted our further studies to the D-*e* and the L-*t* analogs of BODIPY™-LacCer. The contrast between the internalization mechanisms utilized by these analogs is further illustrated in Fig. 3. First we examined the effect of DN Rab5a on internalization of the two isomers. Rab5a promotes the homotypic fusion of very early endosomes to generate the early endosome compartment. As previously shown (24), expression of DN Rab5a had no effect on the initial internalization of the D-*e*-isomer of the LacCer analog; however, uptake of the L-*t* analog was inhibited by about 60% (Fig. 3, *A* and *B*). We also carried out co-localization studies in which cells were double labeled with BODIPY™-D-*e*- or -L-*t*-LacCer and either fluorescent Tfn or dextran (Fig. 3, *C–E*). In the case of the D-*e* analog and Tfn, there was only about 10–15% overlap of the two markers at an early time point (30 s),

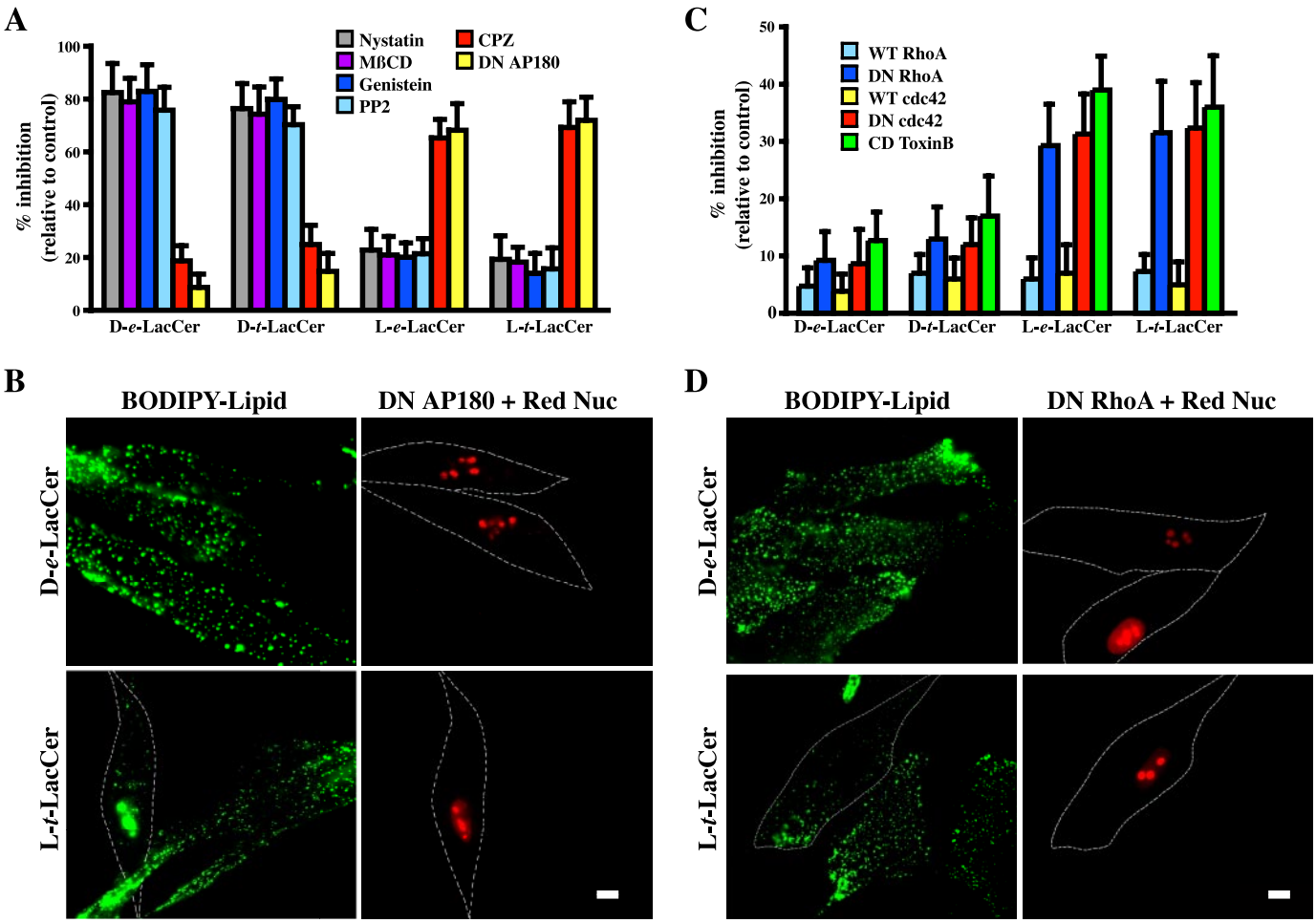

FIGURE 2. **D- and L-stereoisomers of BODIPY™-LacCer are internalized by distinct endocytic mechanisms in HSFs.** *A*, effect of pharmacological inhibitors and DN AP180 on uptake of BODIPY™-LacCer. Cells were pretreated ± the indicated pharmacological inhibitors or co-transfected with DN AP180 and DsRed Nuc constructs. Samples were then incubated with the different BODIPY™-LacCer stereoisomers for 30 min at 10 °C, washed and warmed for 3 min at 37 °C, and then back-exchanged to remove any fluorescent lipid remaining at the PM. Cells were then viewed by fluorescence microscopy and the uptake quantified by image analysis. Percent inhibition is expressed relative to control or untransfected cells. Values are mean ± S.D. of at least 10 cells in each of three independent experiments. *B*, fluorescence micrographs showing the differential endocytosis (3 min at 37 °C) of BODIPY™-D-*e*- *versus* L-*t*-LacCer in HSFs transfected with DN AP180 (*white outlines* indicate transfected cells). Corresponding images of the same cells are shown in *green* (BODIPY™-LacCer) and *red* (to identify cells transfected with DsRed Nuc and DN RhoA). *C*, effect of Rho GTPases on internalization of the BODIPY™-LacCer stereoisomers. Cells were treated with *C. difficile* toxin B or co-transfected with DsRed Nuc and DN RhoA or DN Cdc42. Samples were then pulse-labeled with BODIPY™-LacCer as in *A*, and internalization was quantified. *WT*, wild type. *D*, fluorescence micrographs showing the differential endocytosis (3 min at 37 °C) of BODIPY™-D-*e*- *versus* L-*t*-LacCer in HSFs transfected with DN RhoA (*white outlines* indicate transfected cells). *Bars*, 10 μm.

increasing to about 40% at 3 min. This increase presumably reflects the merging of markers internalized by caveolae and the clathrin pathway at early endosomes (24). In contrast, there was 65–75% overlap of the L-*t* analog with Tfn at all time points examined (0.5–3 min) (Fig. 3*D*). When similar experiments were carried out using the BODIPY™-LacCer analogs and fluorescent dextran, little overlap was seen at any time point using the D-*e* isomer, while ~35% co-localization was seen between L-*t*-LacCer and fluorescent dextran at all times points examined between 0.5 and 3 min (Fig. 3*E*).

Together, the results in Figs. 2 and 3 demonstrate that the D-*e* and D-*t* isomers were internalized by a similar mechanism. Based on our previous studies showing that the D-*e* analog is internalized via caveolae, we conclude that this mechanism also holds for D-*t*-LacCer. In contrast, the L-*e* and L-*t* isomers were internalized primarily by clathrin-dependent endocytosis, with smaller amounts of internalization taking place by RhoA-dependent and Cdc42-dependent mechanisms. However, our data suggest that a small amount of the L-isomers was also internalized *via* caveolae (*e.g.* see Fig. 2*A*).

Organization of BODIPY™-LacCer into PM Domains and Mapping of Endocytic Cargo—We next compared the distribution of BODIPY™-D-*e*- *versus* L-*t*-LacCer at the PM of treated cells. HSFs were incubated with various concentrations of each of these lipids for 30 min at 10 °C, and then images were acquired while maintaining the cells at 10 °C to inhibit endocytosis. To distinguish PM microdomains enriched in LacCer from other regions of the same membrane containing lower concentrations of lipid, we simultaneously monitored both monomer (green) and excimer (red) fluorescence emission (see "Experimental Procedures") (Fig. 4*A*). When low concentrations of BODIPY™-D-*e*-LacCer were used, little heterogeneity in the distribution of the labeled lipid was seen and the PM emitted green fluorescence. When higher concentrations (≥2.5 μM) of the D-*e* analog were used, micron size "patches" of yellow/orange fluorescence were seen on a background of green

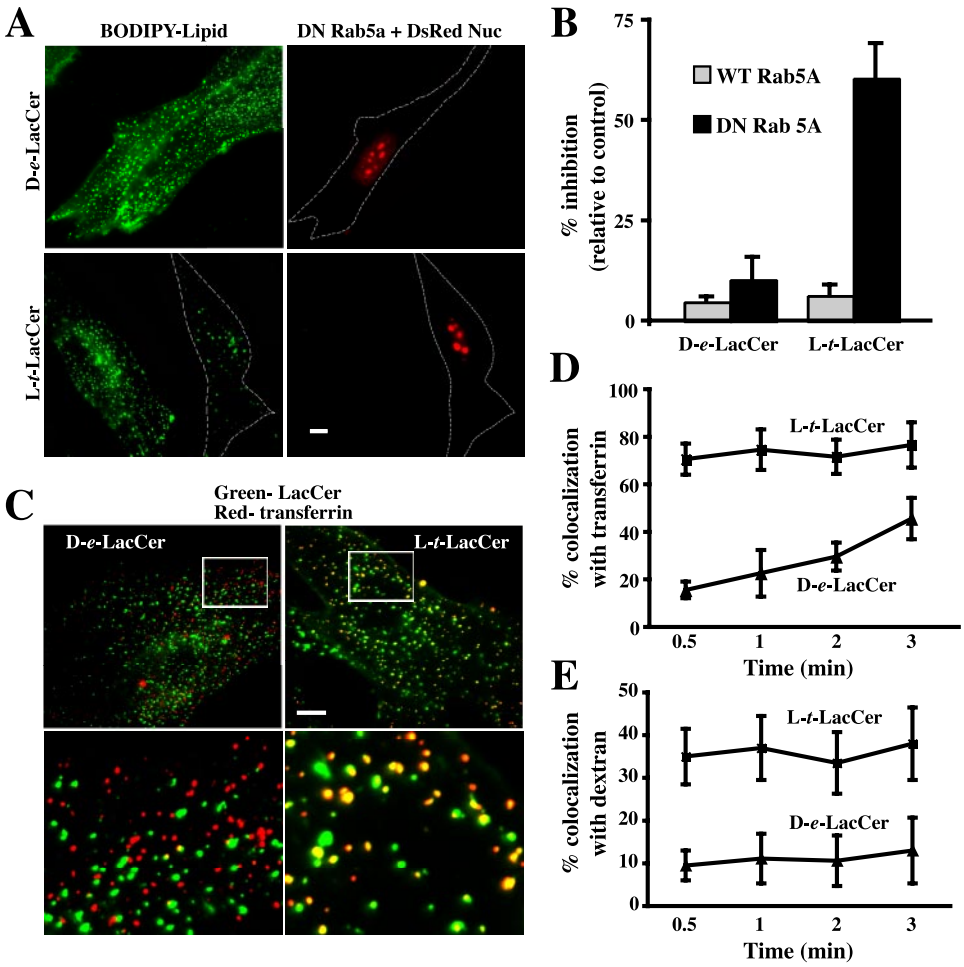

FIGURE 3. **Characterization of the initial endocytosis of BODIPY™-LacCer.** *A* and *B*, effect of DN or wild type (*WT*) Rab5a. HSFs were co-transfected with DsRed Nuc and WT or DN Rab5a. Samples were then pulse labeled with BODIPY™-D-*e versus* L-*t*-LacCer as in Fig. 2*A*. *A*, corresponding images of the same cells are shown in *green* (BODIPY™-LacCer) and *red* (to identify cells transfected with DsRed Nuc and Rab5a). *B*, quantitation of DN Rab5a on the uptake of BODIPY™-LacCer isomers in HSFs. Samples were treated as described for *A*, and uptake was quantified by image analysis. Values are mean ± S.D. of at least 10 cells in each of the three independent experiments. *C* and *D*, co-localization of BODIPY™-LacCer with fluorescent Tfn or dextran. Cells were co-labeled with 1.25 μM BODIPY™-D-*e*- or L-*t*-LacCer (*green*) and 5 μg/ml AF594 Tfn (*red*) (*C*) or 1 mg/ml AF594 dextran (data not shown) for 1 min at 37 °C. In control experiments, no crossover between BODIPY™-LacCer and Tfn or dextran fluorescence was detected using these concentrations of markers. Note the extensive co-localization of BODIPY™-L-*t*-LacCer and Tfn (as seen by the *yellow* endosomes), while for the D-*e* isomer, individual endosomes were either *green* or *red*. In *D* and *E* extent of overlap was quantified between the indicated markers following different periods of co-incubation. *Bars*, 10 μm.

fluorescence at the PM. In contrast, when cells were treated identically, but using BODIPY™-L-*t*-LacCer, only green fluorescence was detected regardless of the concentration used. However, using this analog, we did detect small green patches of fluorescence distributed over the cell surface regardless of the concentration of fluorescent lipid that was used. The absence of excimer fluorescence at the PM of BODIPY™-L-*t*-LacCer-treated cells was not due to decreased incorporation of the L-*t* analog relative to that observed with the D-*e* analog since extraction of the treated cells and quantitative lipid analysis demonstrated that the uptake was approximately the same for both isomers (1744 ± 345 *versus* 1726 ± pmol/mg cell protein for the D-*e versus* L-*t* isomers, respectively).

We next co-incubated cells with BODIPY™-D-*e*- or -L-*t*-LacCer and various fluorescently labeled endocytic markers to map the distribution of these markers on the PM relative to the LacCer microdomains (Fig. 4*B*). β1-Integrin labeled with a Fab fragment overlapped extensively with BODIPY™-D-*e*-LacCer red patches, similar to findings in our previous study (32). No overlap was seen between the green punctae of BODIPY™-L-*t*-LacCer and the β1-integrin Fab fragment (Fig. 4*B*). Little overlap was seen between the clathrin marker, Tfn, and either BODIPY™-D-*e*-LacCer or BODIPY™-L-*t*-LacCer (Fig. 4*C*).

Spectral Properties of BODIPY™-D-e- Versus L-t-LacCer in Lipid Membranes—In an attempt to understand the absence of excimer fluorescence at the PM of cells treated with BODIPY™-L-*t*-LacCer (but not with BODIPY™-D-*e*-LacCer), we examined the spectral properties of the BODIPY™-LacCer stereoisomers in lipid vesicles (Fig. 5). SUVs were prepared by ethanol injection (26, 35) using POPC and 1, 2, 5, or 10 mol % of the fluorescent LacCer analogs and examined by fluorometry using an excitation wavelength of 480 nm. When increasing amounts of BODIPY™-D-*e*-LacCer were incorporated into the vesicles, the intensity of the monomer peak at 515 nm decreased, while there was an increase in excimer emission in the red region (620 nm) (Fig. 5, *A* and *B*), similar to results previously demonstrated for BODIPY™-D-*e*- ceramide (26). In contrast, when BODIPY™-L-*t*-LacCer was used, no excimer shift was seen over this concentration range (Fig. 5, *A* and *B*). In control experiments, the vesicles were lysed with detergent and the total fluorescence was measured at 515 nm to confirm that the same amount of fluorescent lipid had been incorporated into the vesicles for each mol %, regardless of the stereoisomer used (data not shown).

Similarly, when we prepared GUVs containing BODIPY™-D-*e*- and L-*t*-LacCer at the same concentration, GUVs with BODIPY™-D-*e*-LacCer emitted more red fluorescence than GUVs with BODIPY™-L-*t*-LacCer, when viewed by confocal microscopy (Fig. 5*C* and supplemental Fig. 1). Thus, data from both fluorometry and confocal microscopy suggest that the BODIPY™-L-*t*-LacCer monomers have a decreased ability to interact closely with each other and thus exhibit a diminished excimer shift in fluorescence.

Structural Modeling of BODIPY™-LacCer Analogs—We also used chemical modeling programs to generate energy-minimized models of structures of all four stereoisomers of

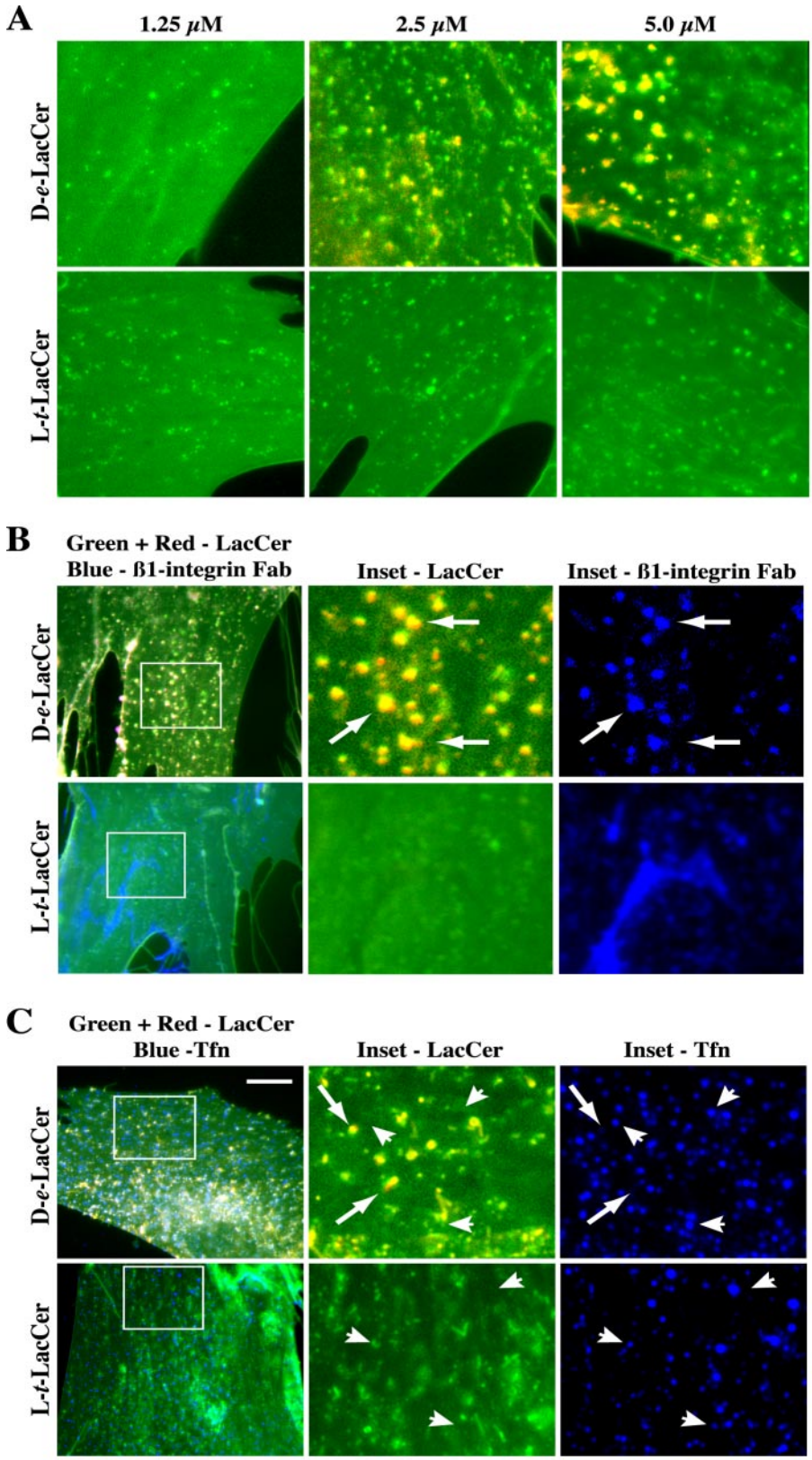

FIGURE 4. **Distribution of BODIPY™-D-*e*- *versus* L-*t*-LacCer at the PM.** *A*, HSFs were incubated with the indicated concentration of BODIPY™-LacCer for 30 min at 10 °C, washed, and observed under the fluorescence microscope at low temperature to inhibit endocytosis. Images were acquired simultaneously at green and red wavelengths (see "Experimental Procedures") and merged. Note the presence of *yellow/orange* micron size patches when BODIPY™-D-*e*-LacCer was used at high concentrations. No such domains were observed using BODIPY™-L-*t*-LacCer. *Bar*, 10 μm. *B* and *C*, mapping endocytic markers to PM domains. HSFs were co-incubated with 5 μM BODIPY™-D-*e*- or L-*t*-LacCer and AF647-labeled anti-β1 integrin Fab (caveolar marker) or AF647-Tfn (clathrin marker) for 30 min at 10 °C. Samples were then observed on the fluorescence microscope at low temperature at green and red wavelengths (BODIPY™-LacCer) and far red wavelengths (endocytic marker). Representative images are shown at low and high magnifications. In corresponding images of the same cell, *arrows* mark the position of BODIPY™-LacCer clusters, while *arrowheads* mark the position of Tfn. *Bars*, 10 μm.

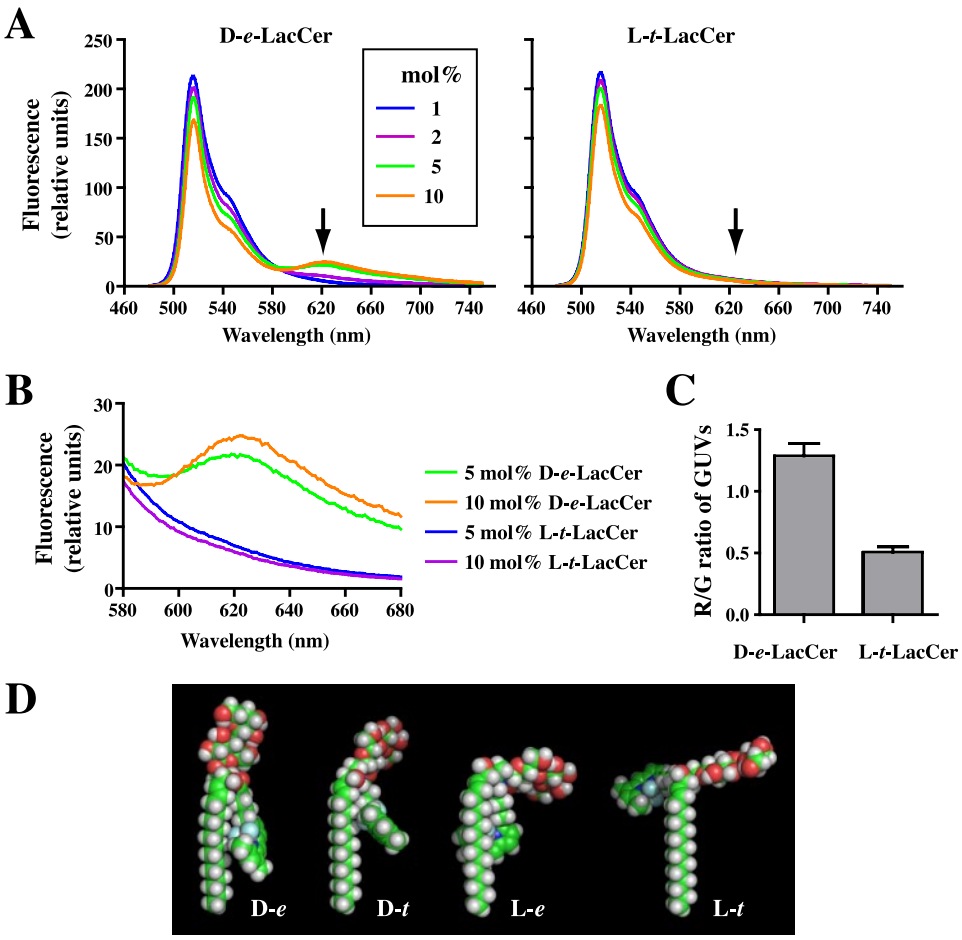

FIGURE 5. **Spectral properties of BODIPY™-LacCer isomers in SUVs and GUVs.** *A*, fluorescence emission spectra of SUVs formed from POPC and containing 1, 2, 5, or 10 mol % BODIPY™-D-*e*-LacCer or -L-*t*-LacCer. Note the presence of monomer (515 nm) and excimer (620 nm; indicated by *arrows*) fluorescence when the D-*e* isomer was used at high mol % fractions. In contrast, no excimer fluorescence was seen under the same conditions using the L-*t* isomer. *B*, plot of fluorescence intensity at long wavelengths for SUVs containing 5 and 10 mol % BODIPY™-D-*e*- or -L-*t*-LacCer. *C*, red/green (*R/G*) fluorescence ratios of GUVs prepared from DOPC/BODIPY™-LacCer/ dipalmitoylphosphatidylglycerol/dilauroylphosphatidylglycerol, 18/2/1/1 mol/mol/mol/mol. GUVs were excited at 488 nm and viewed by confocal microscopy at red and green wavelengths. *D*, molecular models of BODIPY™-LacCer stereoisomers (see "Experimental Procedures").

BODIPY™-LacCer. All structures show a linear hydrocarbon tail attached to the polar sugar head (Fig. 5*D*). In the D-*e* and D-*t* isomers, the sugar rings extend above the sphingosine hydrocarbon chain almost in the same plane whereas in the L-*e* and L-*t* isomers the carbohydrate moiety is nearly perpendicular to the hydrocarbon chain. These differences were further highlighted by rotating the models for the D-*e* and L-*t* isomers in space (see movies in supplemental Fig. 2).

DISCUSSION

We previously showed that BODIPY™-D-*e*-LacCer is internalized almost exclusively by caveolar endocytosis in multiple cell types, including HSFs (7, 8, 11, 17). This was particularly surprising since the LacCer analog appeared to label the PM uniformly and multiple endocytic mechanisms were operative in the cell types we examined. Endocytosis of BODIPY™-D-*e*-LacCer via caveolae was found to be independent of particular carbohydrate headgroups and of sphingosine chain length (8). In the current study we prepared all four possible stereoisomers of BODIPY™-LacCer and investigated their mechanisms of endocytosis. The major findings of our study are (i) the sphingosine stereochemistry dramatically affects the mechanism of LacCer endocytosis, (ii) the natural D-*e* isomer of BODIPY™-LacCer clusters into micron size domains at the PM with increasing concentrations of the lipid, while no such effect is seen using the L-*t* isomer, and (iii) excimer fluorescence is readily detected using high concentrations of the D-*e* (but not L-*t*) isomer of BODIPY™-LacCer, both in cells and in lipid vesicles (SUVs and GUVs). Our findings suggest that the stereochemical orientation of the sphingosine moiety of SLs plays a critical role in the association of these lipids with membrane microdomains.

We first investigated the mechanism of endocytosis of the four stereoisomers. The D-*e* and D-*t* analogs behaved identically to one another and were both selectively internalized *via* caveolae as previously reported for the D-*e* analog (8, 11). The L-*e* and L-*t* isomers also behaved identically to one another, but in contrast to the D-isomers, these analogs were internalized predominantly by clathrin-dependent endocytosis, with additional uptake *via* the RhoA- and Cdc-42-dependent mechanisms. These data suggest that the stereochemistry at a single carbon (C3) of BODIPY™-LacCer regulates its mechanism of internalization (see Fig. 1). To further test this hypothesis we also used (2*S*)-3-deoxy-BODIPY™-LacCer in which the hydroxyl group, and thus the chirality, at C3 is absent. Endocytosis of this compound is inhibited ~80% by chlorpromazine and only 20% by nystatin (see supplemental Fig. 3), indicating its uptake was primarily via clathrin-dependent endocytosis. Thus, loss of the C3 hydroxyl group of BODIPY™-LacCer inhibits uptake via caveolae, providing additional evidence that the stereochemistry at C3 is important for LacCer internalization via caveolae. We also investigated whether our observations could be generalized to other sphingolipids by evaluating the endocytic mechanisms of BODIPY™-D-*e*- *versus* L-*t*-SM. BODIPY™-D-*e*-SM internalization was mainly inhibited by nystatin, whereas that of BODIPY™-L-*t*-SM was inhibited predominantly by chlorpromazine (see supplemental Fig. 3), similar to the results seen with the D-*e*- *versus* L-*t*-isomers of LacCer (Fig. 2). Thus, internalization of SLs via caveolae appears to be regulated mainly by their sphingosine stereochemistry and is not significantly affected by different headgroups (see also Ref. 8).

We then investigated whether the D-*e* and L-*t* analogs pos-

sessed different abilities to cluster into microdomains in the PM of living cells. We found that with increasing concentrations of BODIPY^{TM}-D-*e*-LacCer, the lipid clustered into micron size domains at the PM, which were readily detected by monitoring excimer fluorescence at the cell surface (Fig. 4), similar to our previous studies showing the induction of clustered microdomains by treatment of cells with non-fluorescent, C8-D-*e*-LacCer (32). No clustering of domains was seen using BODIPY^{TM}-L-*t*-LacCer. Importantly, when we attempted to "map" endocytic cargo to the PM domains enriched in BODIPY^{TM}-D-*e*-LacCer, we found that an Fab antibody to β1-integrin co-localized extensively with these domains, while little or no co-localization was seen using fluorescent Tfn, a marker for clathrin-dependent endocytosis (Fig. 4*B*). Interestingly, neither the Fab fragment against β1-integrin nor fluorescent Tfn co-localized with the "green punctae" of BODIPY^{TM}-L-*t*-LacCer at the PM (Fig. 4*B*).

We speculate that the PM domains enriched in fluorescent D-*e*-LacCer may correspond to sites of caveolar endocytosis which will form upon shifting the cells to 37 °C. There are two important consequences of such a scenario. First, the concentration of BODIPY^{TM}-D-*e*-LacCer in vesicle membranes formed upon scission from the PM is expected to be higher than the bulk concentration of the lipid analog at the PM. Such experiments have previously been carried out in our laboratory using BODIPY^{TM}-D-*e*-SM (25), a lipid analog that is internalized at least in part through caveolae (7), and are consistent with this hypothesis. In those experiments, we found that the average value of the fluorescence ratio (red (excimer)/green (monomer)) in endosomes after 7 s of endocytosis was higher than the value of this ratio at the PM prior to endocytosis (25). Second, while these data demonstrate that the D-*e* isomer may be selectively recruited to future sites of caveolar uptake, they do not explain the absence of internalization of this isomer *via* other mechanisms (*e.g.* the clathrin pathway). At present we speculate that an additional unknown "exclusion mechanism" is required to minimize uptake of the natural GSL isomer by non-caveolar endocytosis. This idea is consistent with a report demonstrating that G_{M1} ganglioside is depleted in clathrin-coated pits (36).

In vitro studies with lipid vesicles and molecular modeling revealed a possible explanation for why BODIPY^{TM}-L-*t*-LacCer does not partition into PM microdomains. When we incorporated varying amounts of BODIPY^{TM}-D-*e*-LacCer into unilamellar lipid vesicles formed from DOPC, we found that both monomer ($\lambda_{max} \sim 515$ nm) and excimer ($\lambda_{max} \sim 620$ nm) fluorescence were readily detected using 5–10 mol % of the lipid analog. In contrast, when we used BODIPY^{TM}-L-*t*-LacCer at the same concentrations, very little excimer formation was observed (Fig. 5, *A* and *B*). Similarly, unlike the case for BODIPY^{TM}-D-*e*-LacCer, no red excimer fluorescence was detected in GUVs containing L-*t*-LacCer (Fig. 5*C*). The molecular models shown in Fig. 5*D* suggest that as a result of the different orientation of BODIPY^{TM}-LacCer isomers, the "distance of closest approach" may be greater for the L-*t* isomer than for the D-*e* isomer. Since excimer formation requires close apposition of fluorophores, restricting this approach should reduce the extent of excimer emission. Together, our *in vivo* and *in vitro* data suggest that L-isomers of LacCer are unable to pack as closely to each other and to endogenous SLs as are the D-stereoisomers. This feature may explain their inability to cluster in microdomains and thus be internalized via caveolae.

Finally, our results have important implications for the molecular mechanisms by which SLs become associated with lipid microdomains. Several theories have been proposed to explain the enrichment of SLs in liquid-ordered microdomains. First, it has been proposed that SLs associate with such microdomains as a result of the ability of their saturated acyl chains to tightly pack (37–39). However, in a previous study, we modified the length of the sphingosine base (from 12 to 20 carbons), and the acyl spacer for the fluorescent fatty acid in BODIPY^{TM}-D-*e*-LacCer and found no differences in selective internalization by caveolae for these analogs (8). Furthermore, in the current study, both the D-*e*- and the L-*t* isomers of BODIPY^{TM}-LacCer possess identical fluorescent fatty acids and sphingosine moieties of the same chain length, and yet only the D-*e* analogs associates with microdomains and is internalized via caveolae. Thus, long, saturated acyl chains do not appear to be an essential factor in the association of SL analogs with microdomains, although they may be important for natural SLs. It has also been proposed that SLs may self-associate on the basis of hydrogen-bonding interactions between sphingosine groups (*e.g.* amido/hydroxy interactions) and/or carbohydrate headgroups (39–41). Our observation that alteration of the stereochemistry at C3 of sphingosine perturbs the ability of a LacCer analog to partition into microdomains and to be internalized via caveolae lends support to the idea that the sphingosine moiety is involved in specific SL-SL interactions. The altered structure of L-*t*-LacCer could likely interfere with its ability to form hydrogen bonds involving the C3 hydroxyl group. Because of the drastically altered angle of its lactosyl group (see Fig. 5*D* and supplemental Fig. 2), L-*t*-LacCer may also have a reduced ability to interact with neighboring carbohydrate chains. These findings demonstrate the importance of the configuration at C3 of the sphingosine moiety for the association of SLs with lipid microdomains.

REFERENCES

1. Kirkham, M., Fujita, A., Chadda, R., Nixon, S. J., Kurzchalia, T. V., Sharma, D. K., Pagano, R. E., Hancock, J. F., Mayor, S., and Parton, R. G. (2005) *J. Cell Biol.* **168,** 465–476
2. Mineo, C., and Anderson, R. G. (2001) *Histochem. Cell Biol.* **116,** 109–118
3. Pelkmans, L., and Helenius, A. (2002) *Traffic* **3,** 311–320
4. Cheng, Z. J., Singh, R. D., Marks, D. L., and Pagano, R. E. (2006) *Mol. Membr. Biol.* **23,** 101–110
5. Henley, J. R., Krueger, E. W., Oswald, B. J., and McNiven, M. A. (1998) *J. Cell Biol.* **141,** 85–99
6. Oh, P., McIntosh, D. P., and Schnitzer, J. E. (1998) *J. Cell Biol.* **141,** 101–104
7. Puri, V., Watanabe, R., Singh, R. D., Dominguez, M., Brown, J. C., Wheatley, C. L., Marks, D. L., and Pagano, R. E. (2001) *J. Cell Biol.* **154,** 535–547
8. Singh, R. D., Puri, V., Valiyaveettil, J. T., Marks, D. L., Bittman, R., and Pagano, R. E. (2003) *Mol. Biol. Cell* **14,** 3254–3265
9. Pelkmans, L., Fava, E., Grabner, H., Hannus, M., Habermann, B., Krausz, E., and Zerial, M. (2005) *Nature* **436,** 78–86
10. Schnitzer, J. E., Oh, P., Pinney, E., and Allard, J. (1994) *J. Cell Biol.* **127,** 1217–1232
11. Sharma, D. K., Brown, J. C., Choudhury, A., Peterson, T. E., Holicky, E., Marks, D. L., Simari, R., Parton, R. G., and Pagano, R. E. (2004) *Mol. Biol.*

Cell **15,** 3114–3122
12. Norkin, L. C. (1999) *Immunol. Rev.* **168,** 13–22
13. Pelkmans, L., Kartenbeck, J., and Helenius, A. (2001) *Nat. Cell Biol.* **3,** 473–483
14. Lencer, W. I., Hirst, T. R., and Holmes, R. K. (1999) *Biochim. Biophys. Acta* **1450,** 177–190
15. Orlandi, P. A., and Fishman, P. H. (1998) *J. Cell Biol.* **141,** 905–915
16. Torgersen, M. L., Skretting, G., van Deurs, B., and Sandvig, K. (2001) *J. Cell Sci.* **114,** 3737–3742
17. Cheng, Z. J., Singh, R. D., Sharma, D. K., Holicky, E. L., Hanada, K., Marks, D. L., and Pagano, R. E. (2006) *Mol. Biol. Cell* **17,** 3197–3210
18. Martin, O. C., and Pagano, R. E. (1994) *J. Cell Biol.* **125,** 769–781
19. Liu, Y., and Bittman, R. (2006) *Chem. Phys. Lipids* **142,** 58–69
20. Bittman, R., Kasireddy, C. R., Mattjus, P., and Slotte, J. P. (1994) *Biochemistry* **33,** 11776–11781
21. He, L., Wanunuy, M., Byun, H.-S., and Bittman, R. (1999) *J. Org. Chem.* **64,** 6049–6055
22. Amvam-Zollo, P. H., and Sinay, P. (1986) *Carbohydr. Res.* **150,** 199–212
23. Koval, M., and Pagano, R. E. (1989) *J. Cell Biol.* **108,** 2169–2181
24. Sharma, D. K., Choudhury, A., Singh, R. D., Wheatley, C. L., Marks, D. L., and Pagano, R. E. (2003) *J. Biol. Chem.* **278,** 7564–7572
25. Chen, C. S., Martin, O. C., and Pagano, R. E. (1997) *Biophys. J.* **72,** 37–50
26. Pagano, R. E., Martin, O. C., Kang, H. C., and Haugland, R. P. (1991) *J. Cell Biol.* **113,** 1267–1279
27. Ishitsuka, R., Yamaji-Hasegawa, A., Makino, A., Hirabayashi, Y., and Kobayashi, T. (2004) *Biophys. J.* **86,** 296–307
28. Allinger, N. (1977) *J. Am. Chem. Soc.* **99,** 8127–8134
29. Hehre, W. (2003) *A Guide to Molecular Mechanics and Quantum Chemical Calculations*, pp. 343–356, Wavefunction, Irvine, CA
30. Pietro, W., Francl, M., Hehre, W., DeFrees, D., Pople, J., and Binkley, J. (1982) *J. Am. Chem. Soc.* **104,** 5039–5048
31. Pulay, P. (1982) *J. Comput. Chem.* **3,** 556–560
32. Sharma, D. K., Brown, J. C., Cheng, Z., Holicky, E. L., Marks, D. L., and Pagano, R. E. (2005) *Cancer Res.* **65,** 8233–8241
33. Aktories, K., Schmidt, G., and Just, I. (2000) *Biol. Chem.* **381,** 421–426
34. Sabharanjak, S., Sharma, P., Parton, R. G., and Mayor, S. (2002) *Dev. Cell* **2,** 411–423
35. Kremer, J. M., Esker, M. W., Pathmamanoharan, C., and Wiersema, P. H. (1977) *Biochemistry* **16,** 3932–3935
36. Nichols, B. J. (2003) *Curr. Biol.* **13,** 686–690
37. London, E. (2005) *Biochim. Biophys. Acta* **1746,** 203–220
38. Rajendran, L., and Simons, K. (2005) *J. Cell Sci.* **118,** 1099–1102
39. Wang, T. Y., and Silvius, J. R. (2000) *Biophys. J.* **79,** 1478–1489
40. Masserini, M., and Ravasi, D. (2001) *Biochim. Biophys. Acta* **1532,** 149–161
41. Rietveld, A., and Simons, K. (1998) *Biochim. Biophys. Acta* **1376,** 467–479